Big Data and Information Analytics

https://www.aimspress.com/journal/BDIA

BDIA, 9: 48–67.
DOI:10.3934/bdia.2025003
Received: 22 June 2025
Revised: 06 July 2025
Accepted: 06 August 2025
Published: 12 August 2025

Research article

Quantum ReLU activation function for remote sensing classification and noise robustness analysis

Minghui Yang and Jingli Ren*

School of Mathematics and Statistics, Zhengzhou University, Zhengzhou 450001, China

* **Correspondence:** Email: renjl@zzu.edu.cn.

Abstract: Image classification systems based on convolutional neural networks (CNNs) are frequently subject to noise interruption, and the robustness of CNNs is influenced by the selection of activation functions (AFs). In this paper, we improved the quantum AFs QReLU and m-QReLU, making the parameter value range $0.00001 \leq \alpha \leq 0.01$. We investigated the classification performance and noise robustness of quantum AFs using the EfficientNetB0, DenseNet121, and 2D-CNN models on remote sensing datasets. The experimental results showed that when the quantum AFs parameter is 0.0001, the classification accuracy of the model is higher than that of the ReLU AF. Under UC Merced and WHU RS19 datasets, the classification accuracy of quantum AF increased by 0.52% and 1.65% in the EfficientNetB0 model, and increased by 0.8% and 0.83% in the DenseNet121 model. Under the India Pines dataset, the classification accuracy of quantum AF increased by 1.71%. Furthermore, we individually introduced noise to the remote sensing datasets to investigate the robustness of quantum AFs. The results showed that when the quantum AFs parameter is 0.0001, the model has strong noise robustness.

Keywords: convolutional neural network; quantum computing; noise robustness; activation function; remote sensing classification

1. Introduction

Rapid advances in remote sensing (RS) technology and lower acquisition costs have made vast earth images readily available [1]. RS imagery has gained increasing attention as a research focus [2] and is widely applied in land use and land cover classification [3, 4], flood control [5], crop classification [6], fire prevention [7], gas emission studies [8], and edge detection [9]. Deep learning (DL), the fastest-growing trend in big data analysis and one of 2013's top ten breakthrough technologies [10], has been widespread used in RS applications, particularly convolutional neural networks (CNNs) [11]. Additionally, RS data pose new challenges for DL [10].

A well-trained CNN for image recognition may exhibit significant changes in classification output with minor input modifications [12]. CNNs outperform traditional state-of-the-art techniques in RS image classification, achieving up to 99% accuracy in most scenarios [13, 14]. Training DL models from scratch can lead to overfitting due to added complexity. Deep transfer learning has emerged as a novel framework to address this issue [15, 16], significantly reducing training time and data requirements in the target domain.

RS data often contain noise from natural and human factors, degrading traditional algorithms and requiring robust methods [17]. Hence, boosting the noise robustness of CNNs is vital to RS image classification, with the selection of proper AFs contributing to this goal. AFs in CNNs are crucial for improving model accuracy. CNNs excel at learning hierarchical representations of data, making them well-suited for tasks such as classification, segmentation, and object detection [18] in RS imagery. A well-designed AF is effective in the performance of the DL model [19]. However, there is a lack of consensus on how to select a suitable AF for a neural network model, and a specific one may not be suitable for all applications [20].

Quantum machine learning (QML) is at the crossroads of two of the most exciting current areas of research: quantum computing (QC) and classical machine learning [21]. With QC emerging as a promising platform [22], QML explores how each field's techniques solve the other's problems [23, 24]. The rise of QC has also spurred widespread attention to integrating QC and CNNs for RS image classification. Quantum-inspired machine learning, an emerging field, draws global research attention for its potential to apply quantum mechanics principles in classical computing. Two important concepts in QC are entanglement and superposition. Parisi et al. propose quantum AFs "quantum ReLU" (QReLU) and "modified-QReLU" (m-QReLU) based on quantum entanglement and superposition to address the"dying ReLU" problem [23]. To overcome the issue of "dying ReLU", various AFs such as SELU and PReLU are also proposed. Konar et al. leverage a similar quantum-based sigmoid AF in their quantum-inspired self-supervised network to enhance accuracy and reliability by approximately 1% compared to classical approaches [25].

Here, we investigate the classification performance and noise robustness of CNNs with quantum AFs on RS datasets. This study's major contributions are as follows:

- We improved the quantum AFs QReLU and m-QReLU, making the parameter value range $0.00001 \leq \alpha \leq 0.01$. The parameters of the AFs are determined. When parameter α is 0.0001, the model has the best classification performance.
- We investigate the noise robustness of quantum AFs, and our results show that when the quantum AFs parameter is 0.0001, the model has strong noise robustness.
- We use the t-SNE technique to show the feature distribution of the model. The t-SNE results further demonstrate the rationality of quantum AFs.

2. Datasets and methods

This section comprises the following subsections: Section 2.1 contains the dataset used for classification; Section 2.2 contains the quantum AFs used for classification; Section 2.3 presents DL models and hybrid models used in this study; and Section 2.4 provides performance metrics and hyperparameters used in this study.

2.1. Dataset

We select RS datasets with different visual properties to better evaluate the classification performance and noise robustness.

2.1.1. UC Merced dataset

This manually labeled and publicly available dataset is composed of 2100 aerial scene images with 256×256 pixels, equally divided into 21 land-use classes selected from the United States Geological Survey (USGS) National Map. The 21 categories are agricultural, airplane, baseballdiamond, beach, buildings, chaparral, denseresidential, forest, freeway, golfcourse, harbor, intersection, mediumresidential, mobilehomepark, overpass, parkinglot, river, runway, sparseresidential, storagetanks, and tenniscourt. Some class samples are shown in Figure 1.

2.1.2. WHU RS19 dataset

WHU RS19 dataset [26] contains 1005 high-spatial-resolution images with 600×600 pixels divided into 19 classes, with approximately 50 images per class. This dataset, exported from Google Earth, is more diverse as it includes samples from various parts of the global. There are 19 classes, including airport, beach, bridge, river, forest, meadow, pond, parking, port, viaduct, residential, industrial, commercial, desert, farmland, footballfield, mountain, park, and railwaystation. Some class samples are shown in Figure 2.

2.1.3. India Pines dataset

The Indian Pines image is gathered by the AVIRIS sensor during a flight over the Indian Pines site in Northwestern Indiana. It contains 145×145 pixels and 220 spectral bands in the range of 0.4–2.5 μm. Due to water absorption, 20 spectral bands are removed, and the remaining 200 spectral bands are used for classification. It consists of sixteen land cover classes.

2.2. Quantum activation function

AFs in CNNs play an important role in model accuracy. Exploring the performance of different AFs in CNNs helps to address the gradient vanishing problem and enhance the stability of model training. In large-scale data scenarios, such as RS image classification, exploring the performance of different AFs in RS image classification can provide valuable insights for enhancing model performance. Selecting appropriate AFs for a specific task and dataset can enhance the accuracy and efficiency of the model.

Parisi et al. introduced a quantum computational paradigm to address the unresolved issue of the "dying ReLU" problem in CNNs [23]. This approach aims to solve the "dying ReLU" problem in a quantized way. The proposed approach apply the quantum principles of entanglement and superposition at a computational level to derive two novel AFs: The QReLU and the m-QReLU. QReLU is proposed based on the principle of quantum entanglement, and the formula is

$$QReLU = \begin{cases} x, & \forall x > 0 \\ (\alpha - 2)x, & \forall x \leq 0 \end{cases}, \alpha = 0.01. \tag{2.1}$$

Figure 1. Images for each category in the UC Merced dataset. (a) Agricultural; (b) airplane; (c) baseballdiamond; (d) beach; (e) buildings; (f) chaparral; (g) denseresidential; (h) forest; (i) freeway; (j) golfcourse; (k) harbor; (l) intersection; (m) mediumresidential; (n) mobilehomepark; (o) overpass; (p) parkinglot; (q) river; (r) runway; (s) sparseresidential; (t) storagetanks; and (u) tenniscourt.

m-QReLU is proposed based on the principle of quantum superposition, and the formula is

$$m - QReLU = \begin{cases} x, & \forall x > 0 \\ (\alpha - 1)x, & \forall x \leq 0 \end{cases}, \alpha = 0.01. \tag{2.2}$$

Parameter α takes different values in various classification scenarios due to the differences in data characteristics and other aspects among scenarios. In the classification of RS images, its range is set as α to $0.00001 \leq \alpha \leq 0.01$. This range is determined through experiments, in which different α values are tested, and this interval is derived based on the performance indicators of the model.

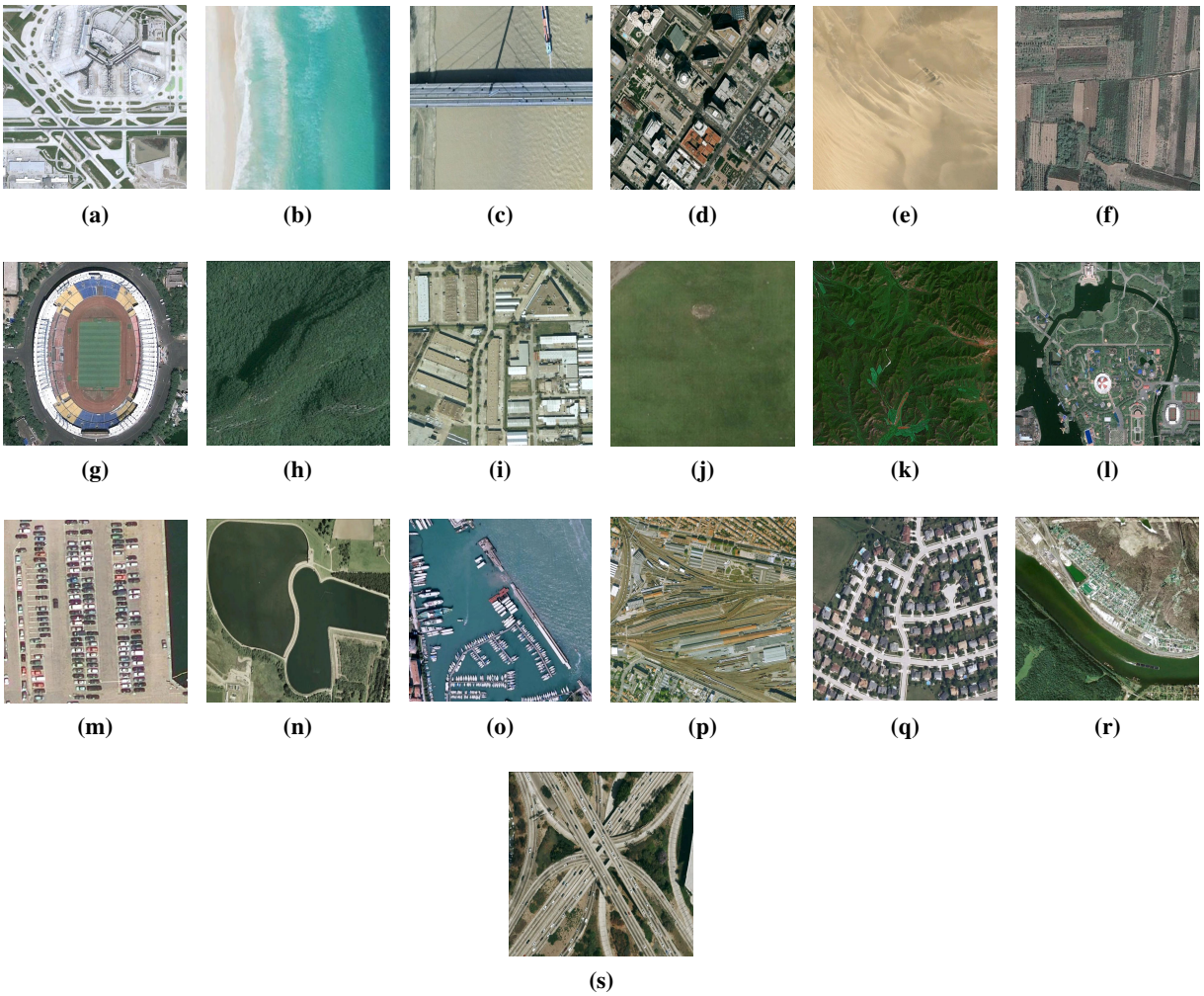

Figure 2. Images for each category in the WHU RS19 dataset. (a) Airport; (b) beach; (c) bridge; (d) commercial; (e) desert; (f) farmland; (g) footballfield; (h) forest; (i) industrial; (j) meadow; (k) mountain; (l) park; (m) parking; (n) pond; (o) port; (p) railwaystation; (q) residential; (r) river; and (s) viaduct.

2.3. Deep learning algorithm and hybrid model

As a typical and important model in the DL community, CNNs construct an end-to-end feature extraction framework, which has achieved excellent performance in RS image recognition tasks [27, 28]. In this section, applied DL algorithms and hyperparameters are given.

2.3.1. EfficientNetB0

EfficientNet is a deep neural network design and scaling method that uses a complicated parameter to evenly scale all depth, width, and resolution variables [29]. The Google Brain team presented the effective CNN model EfficientNet in 2019. The goal of EfficientNet is to improve model performance while taking limited computational resources into account. Unlike current practice, which scales these variables arbitrarily, the EfficientNet scaling approach uses a pre-determined set of scalability variables

to alter network width, depth, and resolution uniformly. EfficientNetB0 is the smallest model in the EfficientNet family.

2.3.2. DenseNet121

DenseNet121 is a CNN-based architecture consisting of 1000-class categories at the beginning, aiming to solve the gradient/information loss problem experienced in DL algorithms by increasing the reuse of features by directly connecting all layers with the feed-forward method, with fewer parameters. In the DenseNet121 architecture, each layer is directly connected to all previous layers. Thus, each layer directly accesses the feature vectors (loss, original input vectors) obtained from all previous layers. Feature vectors obtained from previous layers are combined in a specific layer and used as input. The obtained information (feature vectors, weight vectors) is used as an input vector in all subsequent layers. The architecture consists of 121 convolution layers, 4 dense blocks, 3 transition layers, and a softmax layer in the output layer.

2.3.3. Transfer learning

While huge datasets are typically necessary for the success of networks created from scratch, DL techniques that use pre-trained networks have a lower success rate [7]. In transfer learning applications, DL algorithms are initially trained on a large variety of diverse datasets. The success of the experimental outcomes is then increased by retraining the trained networks using fresh datasets [30].

2.3.4. Hybrid model

We propose a transfer learning approach under the EfficientNetB0 model and the Densenet121 model. The models are fine-tuned, followed by a global average pooling layer and two dense layers. Among them, the feature of the penultimate dense layer is set to 512, and the AFs are QReLU and m-QReLU, respectively. The final dense layer is classified using softmax to analyze the classification of the mixed model on the RS dataset. The transfer learning model is shown in Figure 3(a). Figure 3(b) displays the 2D-CNN model used in this study. We replace the ReLU AF of the first dense layer with QReLU and m-QReLU.

2.4. Performance measures and hyperparameters

2.4.1. Performance measure

The performance of the RS image classification is evaluated using different evaluation metrics, which are as follows :

1) Learning curves: Learning curves are plots used to evaluate the performance of algorithms that incrementally learn from training datasets.
2) Accuracy: Accuracy tells what portion of the images (both positives and negatives of the classifier) are correctly classified. Accuracy is calculated using the following formula:

$$Accuracy = \frac{TP + TN}{TP + TN + FP + FN}. \tag{2.3}$$

TP is the true positive, TN is the true negative, FP is the false positive, and FN is the false negative.

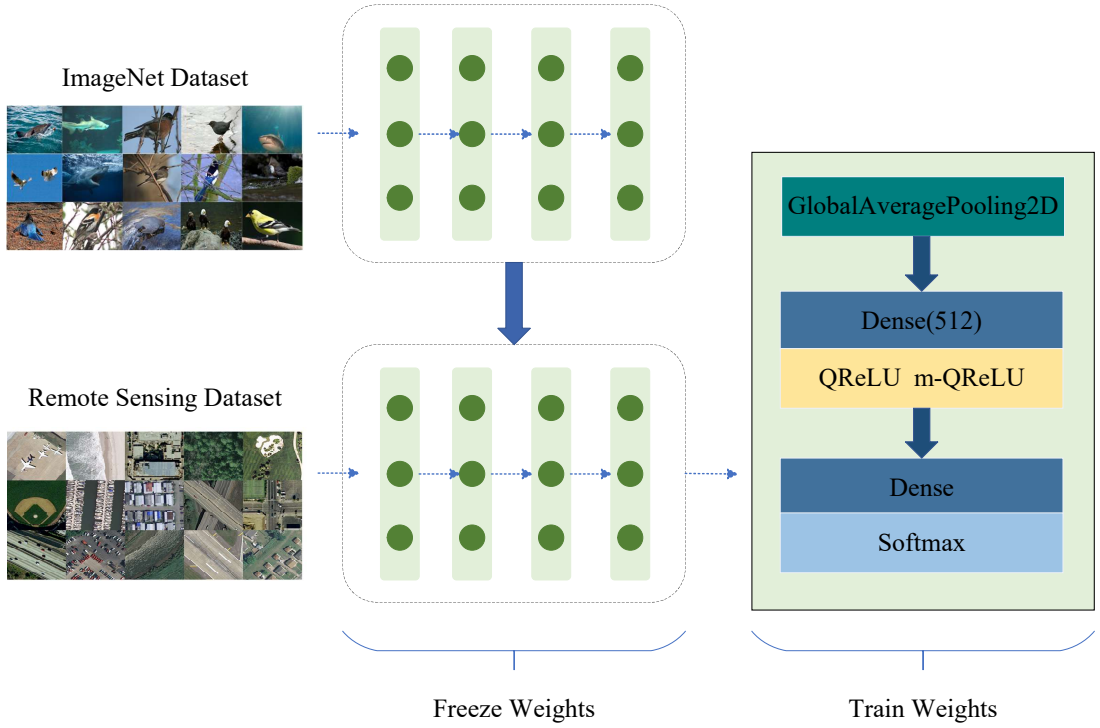

(a) Transfer learning model

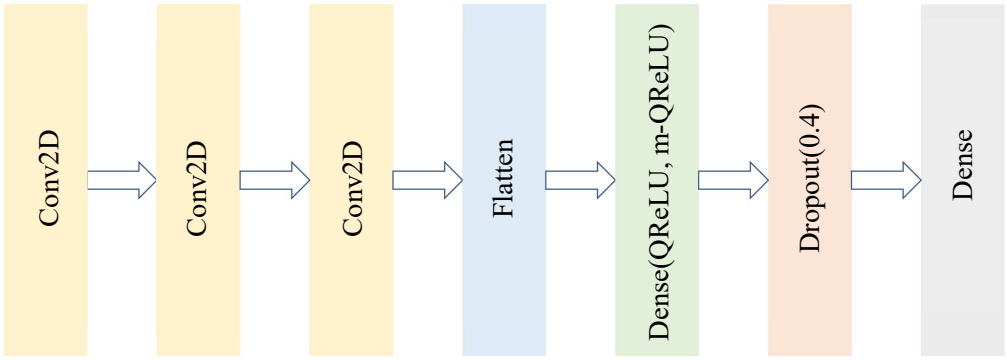

(b) 2D-CNN model

Figure 3. The flowchart of this study.

3) Confusion matrix: Confusion matrix is used for performance evaluation of a machine learning algorithm. It compares the actual values with the predicted classes. Diagonal values of the confusion matrix tell the classification accuracy of each class.
4) Precision: Precision tells what portion of the predicted positives of the classifier is truly positive. Precision is calculated using the following formula:

$$Precision = \frac{TP}{TP + FP}. \tag{2.4}$$

5) Recall: Recall tells what portion of the actual positives of the classifier is correctly classified.

Recall is calculated using the following formula:

$$Recall = \frac{TP}{TP + FN}. \tag{2.5}$$

6) F1-score: The F1-score combines precision and recall into a single value. The F1-Score is obtained by evaluating the harmonic mean of the precision and the recall. F1-Score is calculated using the following formula:

$$F1 - Score = 2 \times \frac{Precision \times Recall}{Precision + Recall}. \tag{2.6}$$

7) Kappa: The Kappa coefficient is an indicator used for testing consistency and can also measure the effectiveness of classification. For a classification problem, consistency refers to whether the model's prediction matches the actual classification result.

2.4.2. Hyperparameters

In this section, the hyperparameters used in the training of deep neural networks are given.

- Training dataset: The training/test ratio in the RS dataset classification study is 6 : 4. The DL algorithms used in the study are trained on the training datasets, and their classification performance are subsequently assessed using test datasets.
- Input shape: The size of the input layer of DL algorithms. In the study, the image input size of all algorithms is determined as $256 \times 256 \times 3$.
- Epoch: Epochs are an important concept in DL model training. Epochs refer to the number of times the complete dataset is fed into the neural network for training. The epoch number is an essential hyperparameter for the DL network to produce successful results in the classification study. In this study, the epoch is chosen as 20.
- Loss function: The goal of the loss function is to minimize the difference between the predicted value and the true value so that the model can make better predictions. In this study, Categorical Cross-entropy, which is frequently used in multi-class classification studies, is used.

$$L_{CCE}(y, \hat{y}) = -\frac{1}{N} \sum_{i=0}^{m} \sum_{j=0}^{n} (y_{ij} * \log(\hat{y}_{ij})), \tag{2.7}$$

  where y represents the true value matrix, $\hat{y}$ the predicted values matrix, and the indices i and j are iterated over the pixel in the image.
- Optimizer: The adam optimization algorithm is used in this study, which is frequently used in optimization studies. The adam optimization aims to accelerate convergence from the beginning of training and continuously reduce the learning rate in training.

3. Remote sensing image classification

The empirical outcomes of hybrid approaches used on the RS datasets are shown in this section. A comparison is made between the classification performance of the CNN model with ReLU, QReLU, and m-QReLU AFs. With a 10 increase, parameter α in QReLU and m-QReLU goes from 0.00001 to

0.01. After many experiments, we determin a parameter $\alpha = 0.0001$, at which quantum AFs have the best classification performance. The numerical result of the experiment is measured three times, and the final result is obtained by averaging. Below, we present the classification results of the model when the quantum AFs parameter is 0.0001.

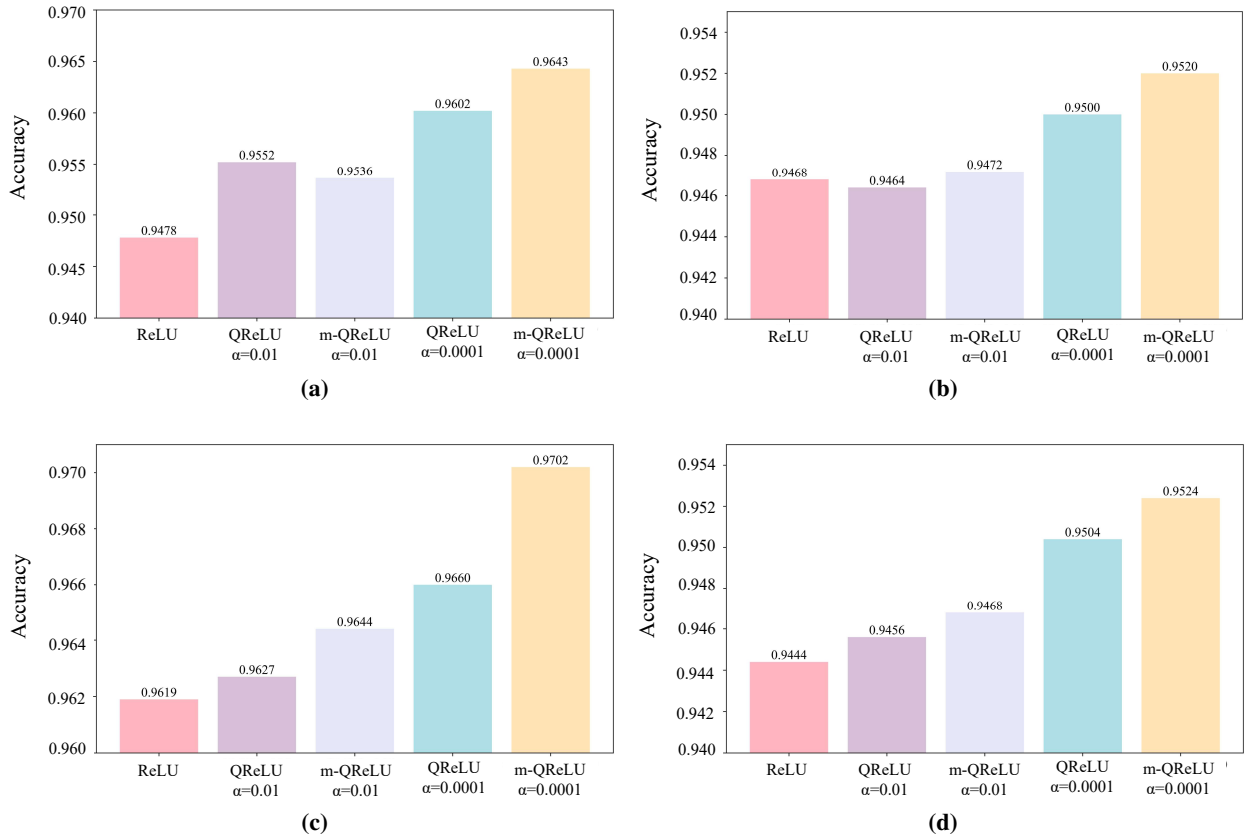

Figure 4. Accuracy of different activation functions. (a),(b) Results of the WHU RS19 and UC Merced datasets on the EfficientNetB0 model. (c),(d) Results of the WHU RS19 and UC Merced datasets on the DenseNet121 model.

3.1. Classification result

3.1.1. Transfer learning model

The performance of the transfer learning models EfficientNetB0 and DenseNet121 in classifying WHU RS19 and UC Merced datasets is illustrated in this section. The classification performance under the QReLU and m-QReLU AFs are summarized in Figure 4. From Figure 4, we know that quantum AFs can improve the model's classification performance of RS datasets.

Figure 4(a) shows the classification result of the WHU RS19 dataset in the EfficientNetB0 model. When the AF is QReLU ($\alpha = 0.0001$), the accuracy reaches 96.02%. When using AF is m-QReLU ($\alpha = 0.0001$), the accuracy achieves 96.43%. The accuracy of QReLU ($\alpha = 0.0001$) AF is 1.24% higher than that of using ReLU, 0.5% higher than QReLU ($\alpha = 0.01$), and 0.66% higher than m-QReLU ($\alpha = 0.01$). The accuracy of m-QReLU ($\alpha = 0.0001$) AF is 1.65% higher than that of using

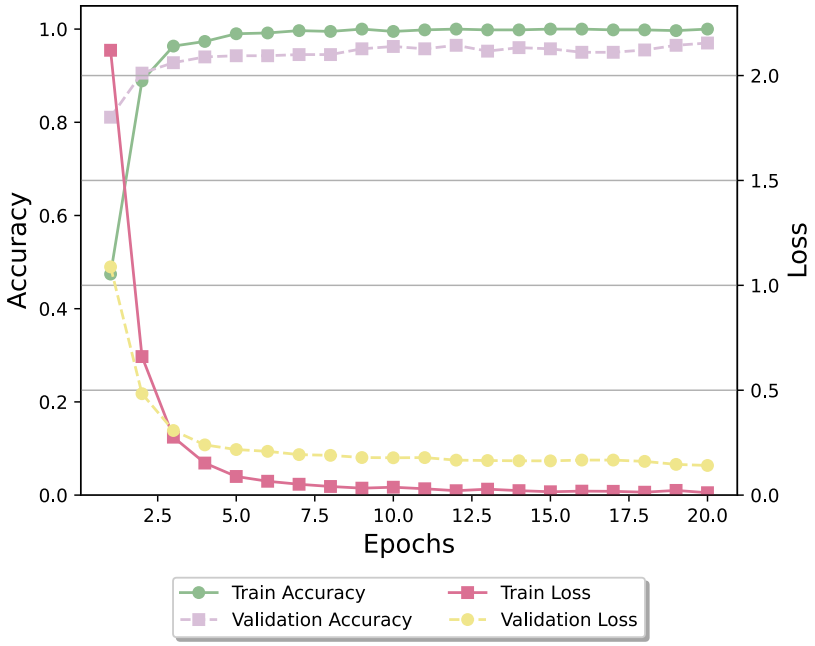

Figure 5. Accuracy and loss curve.

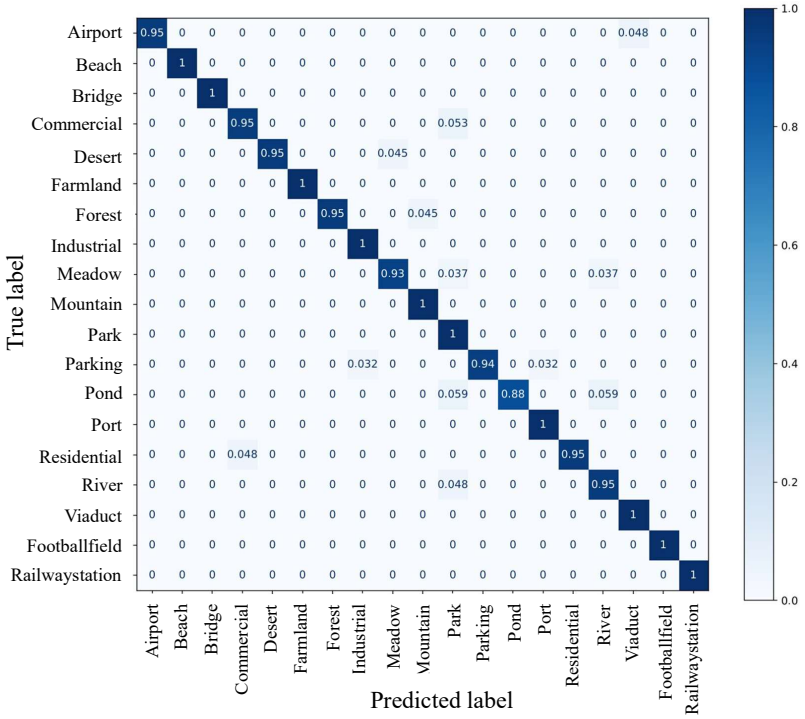

Figure 6. Confusion matrix.

ReLU, 0.91% higher than QReLU ($\alpha = 0.01$), and 1.07% higher than m-QReLU ($\alpha = 0.01$). Figure 5 shows the m-QReLU ($\alpha = 0.0001$) AF's accuracy and loss curve. Figure 6 shows the confusion matrix for classification while using m-QReLU ($\alpha = 0.0001$) AF. Figure 4(b) shows the classification

result of the UC Merced dataset in the EfficientNetB0 model. When the AF is QReLU (α = 0.0001), the accuracy reaches 95.00%. When using AF as m-QReLU (α = 0.0001), the accuracy achieves 95.20%. Figure 4(c) shows the classification result of the WHU RS19 dataset in the DenseNet121 model. When the AF is QReLU (α = 0.0001), the accuracy reaches 96.60%. When using AF as m-QReLU (α = 0.0001), the accuracy achieves 97.02%. Figure 4(d) shows the classification result of the UC Merced dataset in the DenseNet121 model. When the AF is QReLU (α = 0.0001), the accuracy reaches 95.04%. When using AF as m-QReLU (α = 0.0001), the accuracy achieves 95.24%.

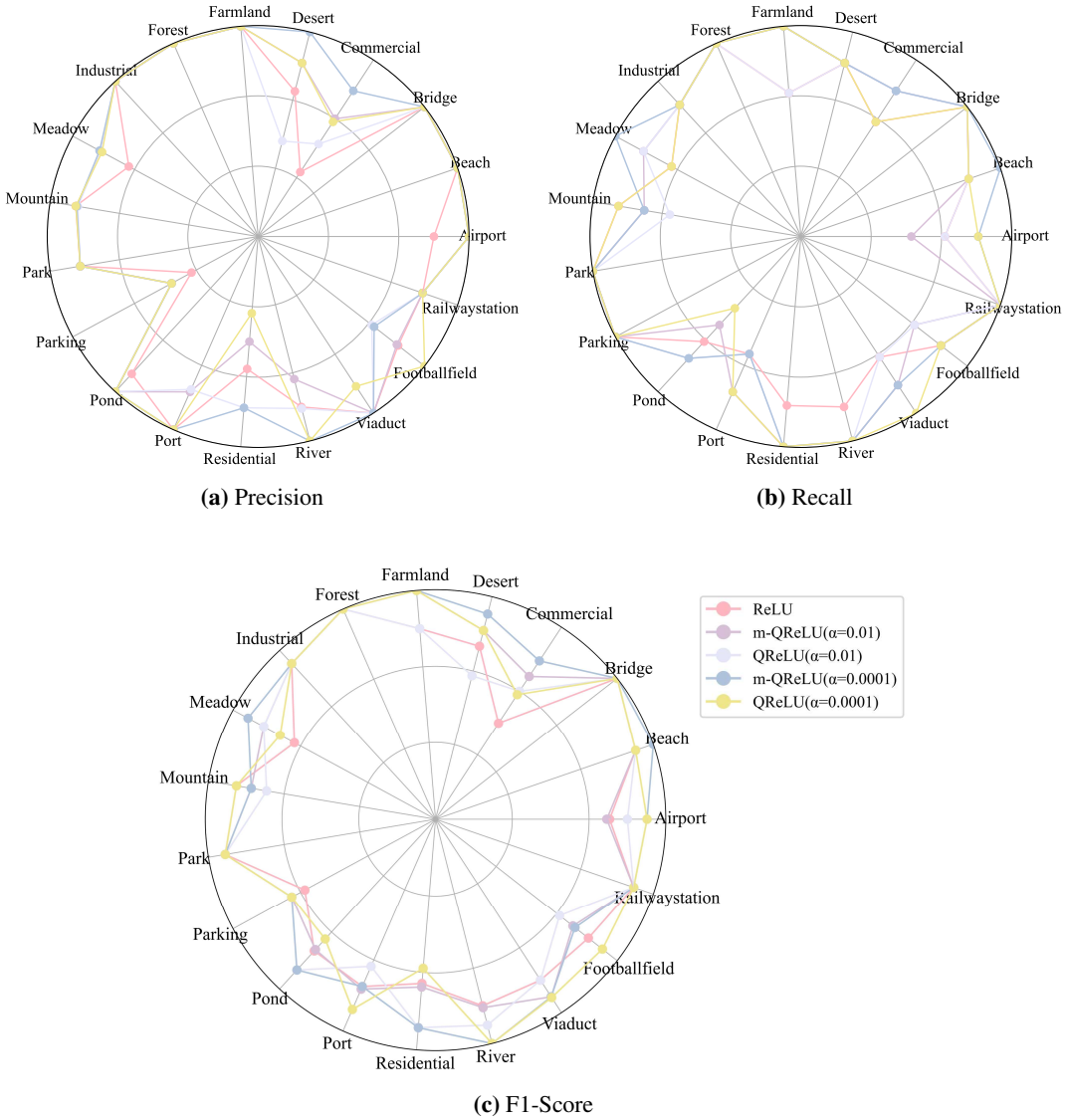

(a) Precision

(b) Recall

(c) F1-Score

Figure 7. Comparison of the Recall, Precision, and F1-Score.

AUC is a widely used metric in fields, such as statistics and machine learning, and is mainly used to evaluate the performance of models, especially the prediction effect of classification models. When classifying the WHU RS19 dataset using EfficientNetB0, the AUC value for QReLU (α = 0.0001) is 0.9982 and for m-QReLU (α = 0.0001) is 0.9984.

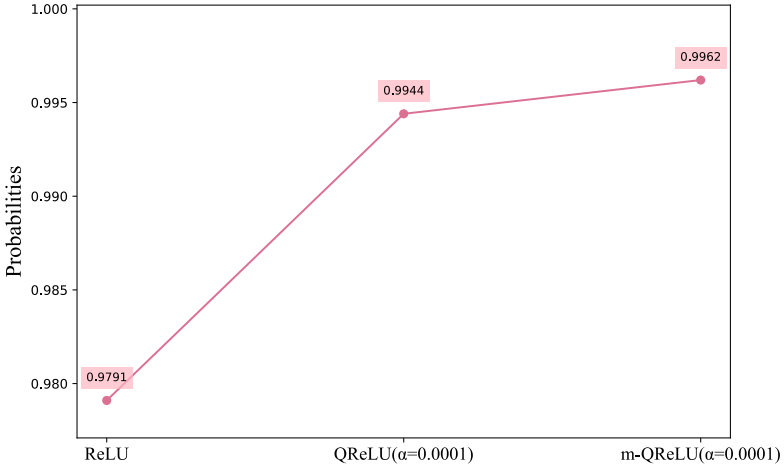

Figure 8. Classification results under the India Pines dataset.

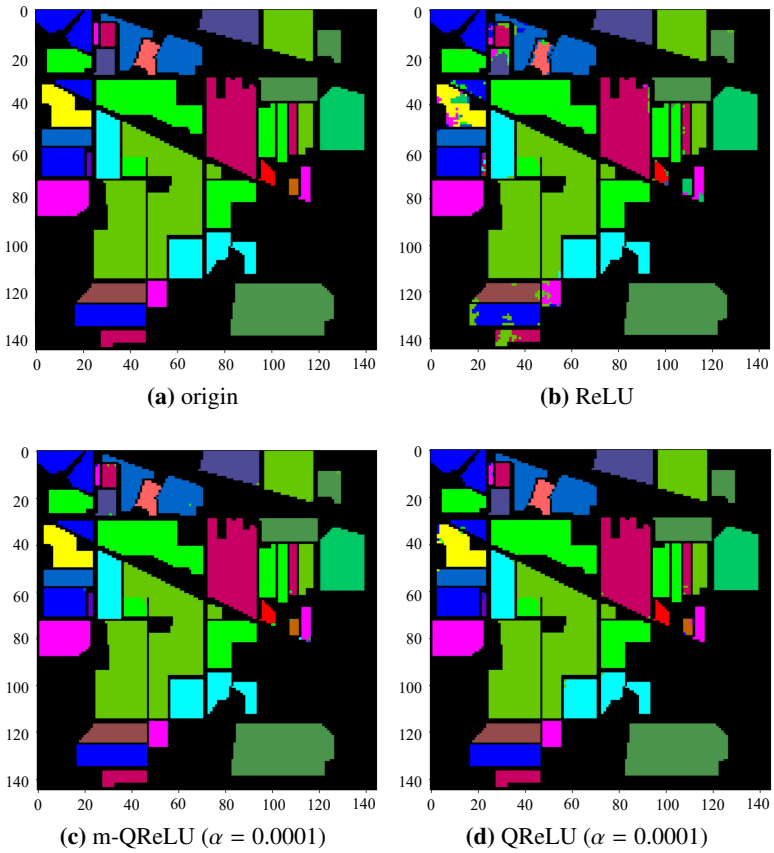

Figure 9. Classification map under the India Pines dataset.

Figure 7 shows the precision, recall, and f1-score values of the EfficientNetB0 model in the WHU RS19 dataset. The innermost probability is 0.7, and as the number of turns increases, the probability increases by 10%.

3.1.2. 2D-CNN model

In this section, we use the 2D-CNN model to classify the India Pines dataset. Figure 8 shows the classification results under the India Pines dataset. When AF is ReLU, the accuracy is 97.91%. When AF is QReLU (α = 0.0001), the accuracy is 99.44%; the accuracy of QReLU (α = 0.0001) AF is 1.53% higher than that of ReLU. When AF is m-QReLU (α = 0.0001), the accuracy is 99.62%; the accuracy of m-QReLU (α = 0.0001) AF is 1.71% higher than that of ReLU. Figure 9 show the classification map of the India Pines dataset. From Figure 9 , we know that the quantum AFs can improve the classification of the RS dataset.

3.2. Visualization of classification results

Figure 10 shows the visualization results of model classification on the UC Merced dataset in the EfficientNetB0 model. Red borders indicate images that have been misclassified. It can be seen from Figure 10 that storagetanks is misclassified as tenniscourt.

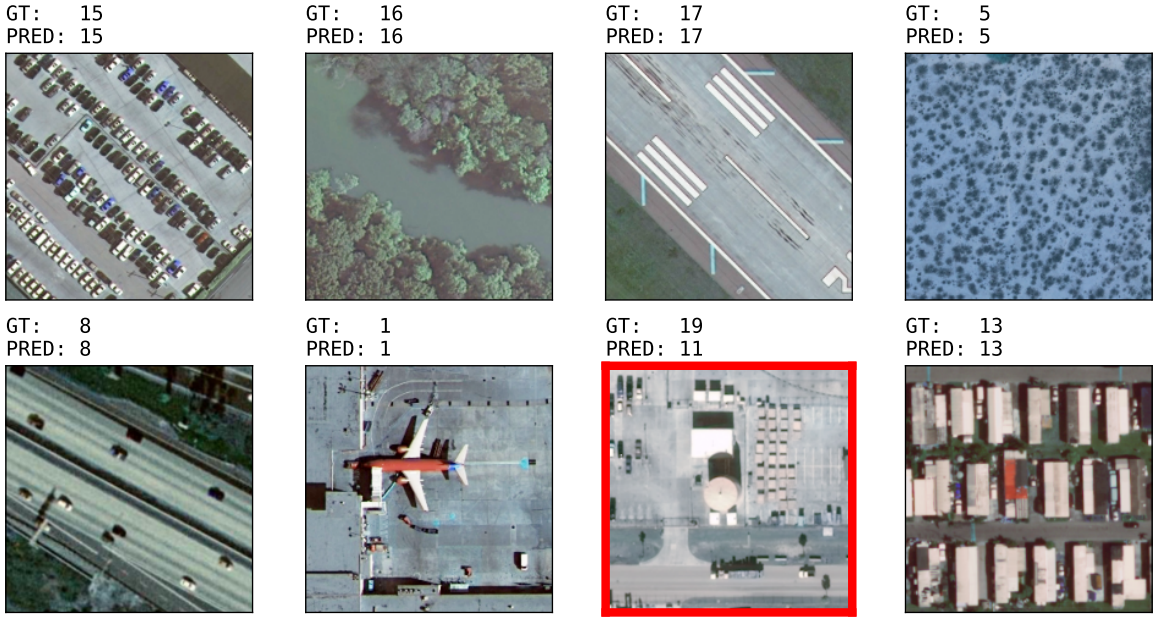

Figure 10. Ground truth and prediction. Agricultural:0, airplane:1, baseballdiamond:2, beach:3, buildings:4, chaparral:5, denseresidential:6, forest:7, freeway:8, golfcourse:9, harbor:10, intersection:11, mediumresidential:12, mobilehomepark:13, overpass:14, parkinglot:15, river:16, runway:17, sparseresidential:18, storagetanks:19, and tenniscourt:20.

In this paper, we use t-distributed stochastic neighbor embedding (t-SNE) to show the feature distribution of the CNN model. t-SNE is a dimensionality reduction technique used to visualize high-dimensional datasets in a two or three-dimensional space. Compared with other dimensionality reduction algorithms, t-SNE creates a reduced feature space where similar samples are represented by nearby points, and dissimilar samples are represented by distant points. Figure 11 show the results of EfficientNetB0 t-SNE visualizations on the WHU RS19 dataset. Different colors represent different categories, with 19 categories in Figure 11. As can be seen from the figure, there are a few

overlapping parts of different colors, which means that very few are misclassified.

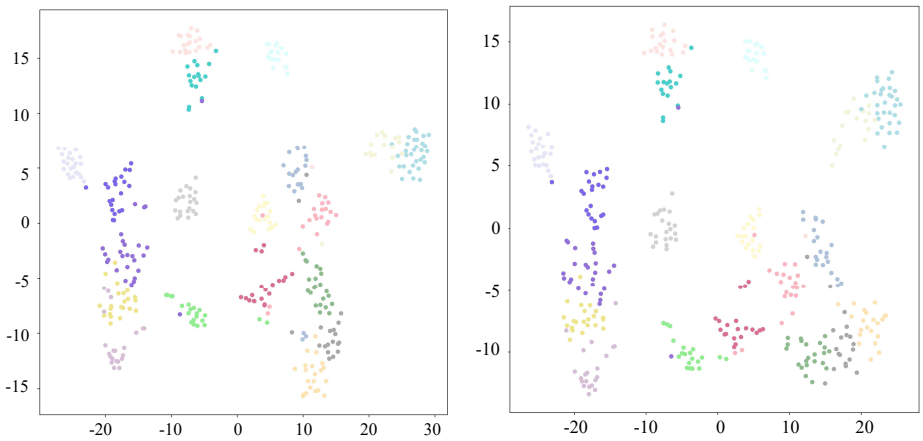

(a) m-QReLU (α = 0.0001) **(b)** QReLU (α = 0.0001)

Figure 11. T-SNE visualization results of the WHU RS19 dataset on the EfficientNetB0 model.

4. Noise robustness analysis

To evaluate the robustness of the quantum AFs, various noises on the RS datasets are used. Three noises are present in the datasets: Salt and Pepper noise, Rayleigh noise, and Gaussian noise. For Gaussian noise, we set the noise intensity to 0.2, the mean of the Gaussian distribution to 0, and the standard deviation to 0.2×225. For Rayleigh noise, the noise intensity is set to 0.2 and scaleparameter is set to 0.2×225. For Salt and Pepper noise, we set the intensity to 0.1, and define 0.5 of the noise points as salt noise and 0.5 as pepper noise. The classification results of different AFs and noises are given in Tables 1 and 2.

Table 1. Classification result of the EfficientNetB0 model in the case of noise.

		ReLU	QReLU $\alpha = 0.01$	m-QReLU $\alpha = 0.01$	QReLU $\alpha = 0.0001$	m-QReLU $\alpha = 0.0001$
WHU RS19	None	0.9478	0.9552	0.9536	0.9602	0.9643
	Gaussian	0.9113	0.9071	0.9105	0.9138	0.9146
	Rayleigh	0.9395	0.9395	0.9395	0.9428	0.9453
	Salt and Pepper	0.9138	0.9129	0.9171	0.9196	0.9204
UC Merced	None	0.9468	0.9464	0.9472	0.9500	0.9520
	Gaussian	0.8909	0.8897	0.8857	0.8964	0.8913
	Rayleigh	0.9127	0.9131	0.9107	0.9190	0.9139
	Salt and Pepper	0.8659	0.8691	0.8734	0.8762	0.8758

Table 1 presents the classification accuracy of the quantum AFs under the EfficientNetB0 model. Under Gaussian noise, quantum AFs (α = 0.0001) achieve an accuracy of 91.46% for the WHU RS19 dataset and 89.64% for the UC Merced dataset. Under Rayleigh noise, the accuracy reaches 94.53%

for the WHU RS19 dataset and 91.90% for the UC Merced dataset. When subjected to Salt and Pepper noise, the accuracy of quantum AFs ($\alpha = 0.0001$) reaches 92.04% for the WHU RS19 dataset and 87.62% for the UC Merced dataset.

Table 2. Classification result of the DenseNet121 model in the case of noise.

		ReLU	QReLU $\alpha = 0.01$	m-QReLU $\alpha = 0.01$	QReLU $\alpha = 0.0001$	m-QReLU $\alpha = 0.0001$
WHU RS19	None	0.9619	0.9627	0.9644	0.9660	0.9702
	Gaussian	0.9246	0.9246	0.9254	0.9270	0.9295
	Rayleigh	0.9527	0.9519	0.9519	0.9544	0.9577
	Salt and Pepper	0.9187	0.9171	0.9221	0.9246	0.9254
UC Merced	None	0.9444	0.9456	0.9468	0.9504	0.9524
	Gaussian	0.8925	0.8829	0.8912	0.8968	0.8976
	Rayleigh	0.9143	0.9107	0.9151	0.9175	0.9198
	Salt and Pepper	0.8738	0.8778	0.8818	0.8833	0.8873

Table 2 presents the classification accuracy of quantum AFs under the DenseNet121 model. Under the WHU RS19 dataset, the quantum AFs ($\alpha = 0.0001$) under Gaussian noise achieve an accuracy of 92.95%; under Rayleigh noise, the quantum AFs ($\alpha = 0.0001$) can achieve an accuracy of 95.77%, while under Salt and Pepper noise, the accuracy of the quantum AFs ($\alpha = 0.0001$) can reach 92.54%. In the UC Merced dataset, the accuracy of the AFs ($\alpha = 0.0001$) under Gaussian noise increases to 89.76%; under Rayleigh noise, the quantum AFs ($\alpha = 0.0001$) achieve an accuracy of 91.98%; while with Salt and Pepper noise, the accuracy can reach 88.73%.

Table 3. Kappa coefficient under the DenseNet121 model.

		ReLU	QReLU $\alpha = 0.01$	m-QReLU $\alpha = 0.01$	QReLU $\alpha = 0.0001$	m-QReLU $\alpha = 0.0001$
WHU RS19	None	0.9597	0.9606	0.9623	0.9649	0.9684
	Gaussian	0.9203	0.9203	0.9212	0.9229	0.9255
	Rayleigh	0.9501	0.9492	0.9492	0.9518	0.9553
	Salt and Pepper	0.9142	0.9124	0.9176	0.9203	0.9212
UC Merced	None	0.9416	0.9429	0.9458	0.9479	0.9500
	Gaussian	0.8870	0.8771	0.8867	0.8916	0.8925
	Rayleigh	0.9100	0.9062	0.9108	0.9117	0.9158
	Salt and Pepper	0.8675	0.8716	0.8758	0.8775	0.8816

Figure 12 shows that the classification performance of QReLU ($\alpha = 0.0001$) and m-QReLU ($\alpha = 0.0001$) is superior to that of ReLU under noise condition. This indicates that quantum AFs exhibit the strongest noise robustness.

Table 3 shows the kappa values of the DenseNet121 model in the WHU RS19 and UC Merced datasets. Table 4 shows the kappa values of the EfficientNetB0 model on the WHU RS19 and UC Merced datasets. In the WHU RS19 dataset, in the absence of noise, the highest kappa value is 96.23%; the maximum kappa value under Gaussian noise is 90.96%; under Rayleigh noise, the highest kappa value is 94.22%; and under Salt and Pepper noise, the highest kappa value is 91.63%. Under the UC

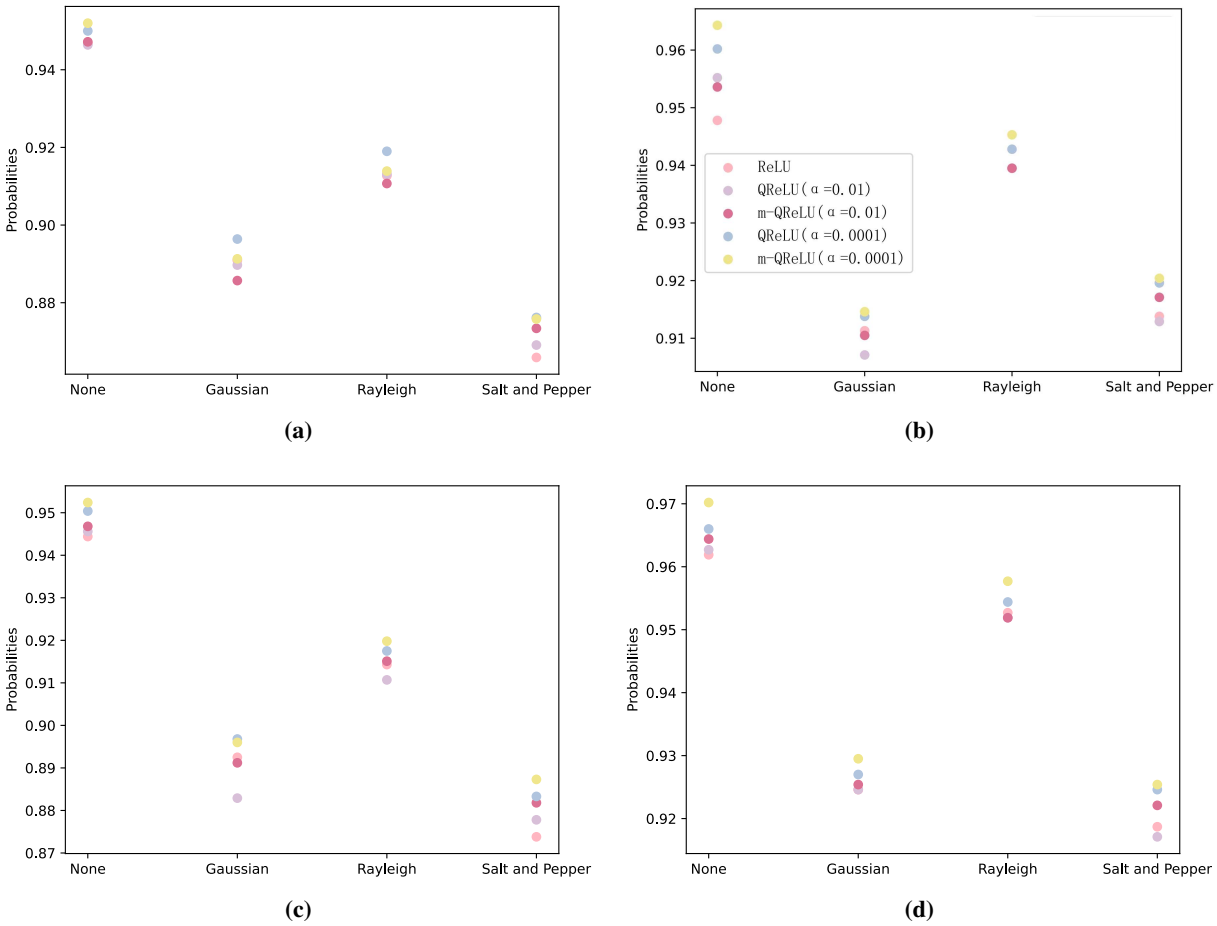

Figure 12. Classification accuracy of different noises. (a),(b) Results of the UC Merced and WHU RS19 datasets on the EfficientNetB0 model. (c),(d) Results of the UC Merced and WHU RS19 datasets on the DenseNet121 model.

Table 4. Kappa coefficient under the EfficientNetB0 model.

		ReLU	QReLU $\alpha = 0.01$	m-QReLU $\alpha = 0.01$	QReLU $\alpha = 0.0001$	m-QReLU $\alpha = 0.0001$
WHU RS19	None	0.9448	0.9527	0.9509	0.9597	0.9623
	Gaussian	0.9063	0.9019	0.9054	0.9089	0.9096
	Rayleigh	0.9361	0.9360	0.9361	0.9396	0.9422
	Salt and Pepper	0.9090	0.9080	0.9126	0.9151	0.9163
UC Merced	None	0.9441	0.9437	0.9445	0.9474	0.9495
	Gaussian	0.8854	0.8841	0.8799	0.8912	0.8858
	Rayleigh	0.9083	0.9087	0.9062	0.9150	0.9096
	Salt and Pepper	0.8591	0.8625	0.8670	0.8700	0.8696

Merced dataset, in the absence of noise, the highest kappa value is 94.95%; the maximum kappa value under Gaussian noise is 89.12%; under Rayleigh noise, the highest kappa value is 91.50%; and under

Salt and Pepper noise, the highest kappa value is 87.00%.

5. Discussion

The success of the application areas of high-parameter and complex deep neural networks is generally proportional to the use of big data [31]. Issues including gradient disappearance, underfitting, and overfitting are now plaguing deep neural networks that are trained on tiny datasets and from scratch [7]. Here, transfer learning can be used to solve these issues. Typically, deeper architectures yield better performance for deep neural networks when offered in application fields.

We use deep neural networks EfficientNetB0 and DenseNet121 in this study, both of which possess high processing power and complex structures. Modern algorithms, such as EfficientNetB0 and DenseNet121, have high parameter values, causing the models to experience an increase in the time elapsed during their training. Moreover, the transfer learning method is used to reduce the time taken during the training of architectures. While huge datasets are typically necessary for the success of networks created from scratch, DL techniques that use pre-trained networks have a lower success rate [7]. In transfer learning applications, DL algorithms are initially trained on a large variety of diverse datasets. Because of its wide range of potential applications, transfer learning has become a hot topic in the field of machine learning [32].

In this study, we explore the implications of researching the noise robustness of CNNs based on different quantum AFs and RS datasets. AFs play a crucial role in introducing non-linearity to CNNs, enabling them to model complex relationships in data. Different AFs exhibit varying properties in terms of their ability to handle noise and promote robustness in CNNs. In the research, a hybrid approach of the DL model and quantum AFs is adopted. Our results show that when the quantum AF parameter is 0.0001, the model classification performance is higher than the classification accuracy of ReLU. In the EfficientNetB0 model, the highest classification accuracy is 95.20% under the UC Merced dataset and 96.43% under the WHU RS19 dataset. In the DenseNet121 model, the highest classification accuracy is 95.24% under the UC Merced dataset and 97.02% under the WHU RS19 dataset. In the 2D-CNN model, the highest classification accuracy under the India Pines dataset is 99.62%. Under noisy RS datasets, the results show that when the quantum AF parameter is 0.0001, the model has strong noise robustness. In general, the quantum AFs are optimal in improving model accuracy and noise robustness.

The findings of research on noise robustness have practical implications for real-world RS applications. Robust CNN models can facilitate more accurate and reliable analysis of RS data, enabling better decision-making in areas such as agriculture, urban planning, disaster response, and environmental monitoring.

6. Conclusions

In this paper, we leverage CNNs and quantum AFs to perform RS scene classification, and analyze noise robustness. Quantum AFs are chosen based on different DL methods to classify the scenes of three benchmark RS datasets.

To evaluate the performance of quantum AFs, a series of experiments are conducted. The results show that when $\alpha = 0.0001$, the performance of quantum AF is superior to that of ReLU AF. The

experimental results demonstrate the effectiveness and robustness of the quantum AFs.

Future research in this area could entail exploring novel AFs designed to address the challenges of noise in RS datasets. Additionally, investigating ensemble methods and hybrid architectures that combine multiple AFs could further enhance the robustness and versatility of CNN models for RS applications.

Use of AI tools declaration

The authors declare they have not used Artificial Intelligence (AI) tools in the creation of this article.

Acknowledgments

This work was supported by the National Key R&D Program of China (No. 2024YFB3411500) and the National Natural Science Foundation of China (No. U23A2065).

Conflict of interest

The authors declare that they have no conflict of interest with respect to the research, authorship, and publication of the article.

References

1. Zhou W, Guan H, Li Z, Shao Z, Delavar MR, (2023) Remote sensing image retrieval in the past decade: Achievements, challenges, and future directions. *IEEE J Sel Top Appl Earth Obs Remote Sens* 16: 1447–1473. https://doi.org/10.1109/JSTARS.2023.3236662
2. Peng C, Li Y, Shang R, Jiao L, (2023) RSBNet: One-shot neural architecture search for a backbone network in remote sensing image recognition. *Neurocomputing* 537: 110–127. https://doi.org/10.1016/j.neucom.2023.03.046
3. Tejasree G, Agilandeeswari L, (2024) Land use/land cover (LULC) classification using deep-LSTM for hyperspectral images. *Egypt J Remote Sens Space Sci* 27: 52–68. https://doi.org/10.1016/j.ejrs.2024.01.004
4. Zhao Z, Islam F, Waseem LA, Tariq A, Nawaz M, Ijaz UI, et al. (2024) Comparison of three machine learning algorithms using google earth engine for land use land cover classification. *Rangel Ecol Manag* 92: 129–137. https://doi.org/10.1016/j.rama.2023.10.007
5. Duan C, Zheng X, Li R, Wu Z, (2024) Urban flood vulnerability knowledge-graph based on remote sensing and textual bimodal data fusion. *J Hydrol* 633: 131010. https://doi.org/10.1016/j.jhydrol.2024.131010
6. Li H, Tian Y, Zhang C, Zhang S, Atkinson PM, (2022) Temporal sequence object-based CNN (TS-OCNN) for crop classification from fine resolution remote sensing image time-series. *Crop J* 10: 1507–1516. https://doi.org/10.1016/j.cj.2022.07.005
7. Reis HC, Turk V, (2023) Detection of forest fire using deep convolutional neural networks with transfer learning approach. *Appl Soft Comput* 143: 110362. https://doi.org/10.1016/j.asoc.2023.110362

8. Zhang S, Ma J, Zhang X, Guo C, (2023) Atmospheric remote sensing for anthropogenic methane emissions: Applications and research opportunities. *Sci Total Environ* 893: 164701. https://doi.org/10.1016/j.scitotenv.2023.164701
9. Du Y, Song W, He Q, Huang D, Liotta A, Su C, (2019) Deep learning with multi-scale feature fusion in remote sensing for automatic oceanic eddy detection. *Inform Fusion* 49: 89–99. https://doi.org/10.1016/j.inffus.2018.09.006
10. Zhu XX, Tuia D, Mou L, Xia GS, Zhang L, Xu F, (2017) Deep learning in remote sensing: A comprehensive review and list of resources. *IEEE Geosci Remote Sens Mag* 5: 8–36. https://doi.org/10.1109/MGRS.2017.2762307
11. Jozdani S, Chen D, Pouliot D, Johnson BA, (2022) A review and meta-analysis of generative adversarial networks and their applications in remote sensing. *Int J Appl Earth Obs Geoinf* 108: 102734. https://doi.org/10.1016/j.jag.2022.102734
12. Konar D, Sarma A D, Bhandary S, Bhattacharyya S, Cangi A, Aggarwal V, (2023) A shallow hybrid classical-quantum spiking feedforward neural network for noise-robust image classification. *Appl Soft Comput* 136: 110099. https://doi.org/10.1016/j.asoc.2023.110099
13. Zhong Z, Li J, Luo Z, Chapman M, (2017) Spectral-spatial residual network for hyperspectral image classification: A 3-D deep learning framework. *IEEE Trans Geosci Remote Sens* 56: 847–858. https://doi.org/10.1109/TGRS.2017.2755542
14. Roy SK, Krishna G, Dubey SR, Chaudhuri BB, (2019) HybridSN: Exploring 3-D-2-D CNN feature hierarchy for hyperspectral image classification. *IEEE Geosci Remote Sens Lett* 17: 277–281. https://doi.org/10.1109/LGRS.2019.2918719
15. Naushad R, Kaur T, Ghaderpour E, (2021) Deep transfer learning for land use and land cover classification: A comparative study. *Sens Basel* 21: 8083. https://doi.org/10.3390/s21238083
16. Zhang H, Jiang Z, Zheng G, Yao X, (2023) Semantic segmentation of high-resolution remote sensing images with improved U-Net based on transfer learning. *Int J Comput Int Sys* 16: 181. https://doi.org/10.1007/s44196-023-00364-w
17. Zhang Q, Xiao J, Tian C, Lin JCW, Zhang S, (2022) A robust deformed convolutional neural network (CNN) for image denoising. *Caai T Intell Techno* 8: 331–342. https://doi.org/10.1049/cit2.12110
18. Sagar ASMS, Chen Y, Xie YK, Kim HS, (2024) MSA R-CNN: A comprehensive approach to remote sensing object detection and scene understanding. *Expert Syst Appl* 241: 122788. https://doi.org/10.1016/j.eswa.2023.122788
19. Kiliçarslan S, Celik M, (2021) RSigELU: A nonlinear activation function for deep neural networks. *Expert Syst Appl* 174: 114805. https://doi.org/10.1016/j.eswa.2021.114805
20. Liew SS, Khalil-Hani M, Bakhteri R, (2016) Bounded activation functions for enhanced training stability of deep neural networks on visual pattern recognition problems. *Neurocomputing* 216: 718–734. https://doi.org/10.1016/j.neucom.2016.08.037
21. Shi S, Wang Z, Cui G, Wang S, Shang R, Li W, et al. (2022) Quantum-inspired complex convolutional neural networks. *Appl Intell* 52: 17912–17921. https://doi.org/10.1007/s10489-022-03525-0

22. Wang H, (2024) A novel feature selection method based on quantum support vector machine. *Phys Scripta* 99: 056006. https://doi.org/10.1088/1402-4896/ad36ef
23. Parisi L, Neagu D, Ma R, Campean F, (2022) Quantum ReLU activation for convolutional neural networks to improve diagnosis of Parkinson's disease and COVID-19. *Expert Syst Appl* 187: 115892. https://doi.org/10.1016/j.eswa.2021.115892
24. Peral-García D, Cruz-Benito J, García-Peñalvo FJ, (2024) Systematic literature review: Quantum machine learning and its applications. *Comput Sci Rev* 51: 100619. https://doi.org/10.1016/j.cosrev.2024.100619
25. Konar D, Bhattacharyya S, Gandhi TK, Panigrahi BK, (2020) A quantum-inspired self-supervised network model for automatic segmentation of brain MR images. *Appl Soft Comput* 93: 106348. https://doi.org/10.1016/j.asoc.2020.106348
26. Sheng G, Yang W, Xu T, Sun H, (2012) High-resolution satellite scene classification using a sparse coding based multiple feature combination. *Int J Remote Sens* 33: 2395–2412. https://doi.org/10.1080/01431161.2011.608740
27. Zhu D, Xia S, Zhao J, Zhou Y, Jian M, Niu Q, et al. (2020) Diverse sample generation with multi-branch conditional generative adversarial network for remote sensing objects detection. *Neurocomputing* 381: 40–51. https://doi.org/10.1016/j.neucom.2019.10.065
28. Li C, Cong R, Guo C, Li H, Zhang C, Zheng F, et al. (2020) A parallel down-up fusion network for salient object detection in optical remote sensing images. *Neurocomputing* 415: 411–420. https://doi.org/10.1016/j.neucom.2020.05.108
29. Papoutsis I, Bountos N I, Zavras A, Michail D, Tryfonopoulos C, (2023) Benchmarking and scaling of deep learning models for land cover image classification. *ISPRS J Photogramm Remote Sens* 195: 250–268. https://doi.org/10.1016/j.isprsjprs.2022.11.012
30. Bouguettaya A, Zarzour H, Taberkit AM, Kechida A, (2022) A review on early wildfire detection from unmanned aerial vehicles using deep learning-based computer vision algorithms. *Signal Process* 190: 108309. https://doi.org/10.1016/j.sigpro.2021.108309
31. Rajpurkar P, Park A, Irvin J, Chute C, Bereket M, Mastrodicasa D, et al. (2020) AppendiXNet: Deep learning for diagnosis of appendicitis from a small dataset of CT exams using video pretraining. *Sci Rep* 10: 3958. https://doi.org/10.1038/s41598-020-61055-6
32. Zhuang F, Qi Z, Duan K, Xi D, Zhu Y, Zhu H, et al. (2020) A comprehensive survey on transfer learning. *Proc IEEE* 109: 43–76. https://doi.org/10.1109/JPROC.2020.3004555

AIMS Press